Available online at www.sciencedirect.com

ScienceDirect

Nuclear Physics B 878 (2014) 295–308

NUCLEAR PHYSICS B

www.elsevier.com/locate/nuclphysb

Direct detection and solar capture of dark matter with momentum and velocity dependent elastic scattering

Wan-Lei Guo [a,*], Zheng-Liang Liang [a,b], Yue-Liang Wu [a,b]

[a] *State Key Laboratory of Theoretical Physics (SKLTP), Kavli Institute for Theoretical Physics China (KITPC), Institute of Theoretical Physics, Chinese Academy of Science, Beijing 100190, China*

[b] *University of Chinese Academy of Sciences, Beijing 100049, China*

Received 26 September 2013; accepted 26 November 2013

Available online 1 December 2013

Abstract

We explore the momentum and velocity dependent elastic scattering between the dark matter (DM) particles and the nuclei in detectors and the Sun. In terms of the non-relativistic effective theory, we phenomenologically discuss ten kinds of momentum and velocity dependent DM–nucleus interactions and recalculate the corresponding upper limits on the spin-independent DM–nucleon scattering cross section from the current direct detection experiments. The DM solar capture rate is calculated for each interaction. Our numerical results show that the momentum and velocity dependent cases can give larger solar capture rate than the usual contact interaction case for almost the whole parameter space. On the other hand, we deduce the Super-Kamiokande's constraints on the solar capture rate for eight typical DM annihilation channels. In contrast to the usual contact interaction, the Super-Kamiokande and IceCube experiments can give more stringent limits on the DM–nucleon elastic scattering cross section than the current direct detection experiments for several momentum and velocity dependent DM–nucleus interactions. In addition, we investigate the mediator mass effect on the DM elastic scattering cross section and solar capture rate.

1. Introduction

The existence of dark matter (DM) is by now well confirmed [1,2]. The recent cosmological observations have helped to establish the concordance cosmological model where the present

* Corresponding author.
E-mail addresses: guowl@itp.ac.cn (W.-L. Guo), liangzl@itp.ac.cn (Z.-L. Liang), ylwu@itp.ac.cn (Y.-L. Wu).

0550-3213
http://dx.doi.org/10.1016/j.nuclphysb.2013.11.016

Universe consists of about 68.3% dark energy, 26.8% dark matter and 4.9% atoms [3]. Understanding the nature of dark matter is one of the most challenging problems in particle physics and cosmology. The DM direct detection experiments may observe the elastic scattering of DM particles with nuclei in detectors. Current and future DM direct search experiments may constrain or discover the DM for its mass m_D and elastic scattering cross section σ_n with nucleon. As well as in the DM direct detection, the DM particles can also elastically scatter with nuclei in the Sun. Then they may lose most of their energy and are trapped by the Sun [1]. It is clear that the DM solar capture rate $C_\odot$ is related to the DM–nucleon elastic scattering cross section σ_n. Due to the interactions of the DM annihilation products in the Sun, only the neutrino can escape from the Sun and reach the Earth. Therefore, the water Cherenkov detector Super-Kamiokande (SK) [4], the neutrino telescopes IceCube (IC) [5,6] and ANTARES [7] can also give the information about m_D and σ_n through detecting the neutrino induced upgoing muons.

The current experimental results about σ_n are based on the standard DM–nucleus contact interaction which is independent of the transferred momentum q and the DM velocity v. In fact, many DM scenarios can induce the momentum and velocity dependent DM–nucleus interactions. For example, the differential scattering cross section of a long-range interaction will contain a factor $(q^2 + m_\phi^2)^{-2}$ with m_ϕ being the mass of a light mediator ϕ [8,9]. It is worthwhile to stress that the current experimental results about σ_n must be recalculated for the momentum and velocity dependent DM–nucleus interactions. In view of this feature, many authors have recently used the momentum and velocity dependent DM–nucleus interactions to reconcile or improve the tension between the DAMA annual modulation signal and other null observations [9–13]. The new upper limit on σ_n can directly affect the maximal $C_\odot$. On the other hand, we have to recalculate $C_\odot$ for a fixed σ_n when the DM–nucleus interaction is dependent on the momentum and velocity. For the usual contact interaction, the current direct search experiment XENON100 [14] provides a more stringent limit on spin-independent (SI) σ_n than the Super-Kamiokande and IceCube experiments when $m_D \gtrsim 10$ GeV [4–6]. We do not know whether this conclusion still holds for the momentum and velocity dependent DM–nucleus interactions. It is very necessary for us to systematically investigate the momentum and velocity dependent DM elastic scattering in detectors and the Sun.

In this paper, we will explore the momentum and velocity dependent DM–nucleus interactions and discuss their effects on the SI σ_n and the DM solar capture rate $C_\odot$. New upper limits on σ_n from the XENON100 [14] and XENON10 [15], and the corresponding maximal $C_\odot$ will be calculated for these interactions. On the other hand, we shall deduce the constraints on $C_\odot$ from the latest Super-Kamiokande results for eight typical DM annihilation channels. In addition, the mediator mass effect on σ_n and $C_\odot$ will also be analyzed. This paper is organized as follows: In Section 2, we outline the main features of the momentum and velocity dependent DM–nucleus interactions in direct detection experiments, and derive the corresponding upper limits on σ_n. In Section 3, we numerically calculate $C_\odot$ for these interactions and give the general constraints on $C_\odot$ from the Super-Kamiokande and IceCube. In Section 4, we discuss the mediator mass effect on σ_n and $C_\odot$. Finally, some discussions and conclusions are given in Section 5.

2. Dark matter direct detection

2.1. DM event rate

The event rate R of a DM detector in the direct detection experiments can be written as

$$R = N_T \frac{\rho_{\rm DM}}{m_D} \int \frac{d\sigma_N}{dE_R} dE_R \int_{v_{\rm min}}^{v_{\rm max}} v f(v)\, d^3 v,$$
$$= N_T \frac{\rho_{\rm DM}}{m_D} \frac{\pi A^2 m_N \sigma_n}{\mu_n^2} \int F_N^2(q)\, dE_R \int_{-1}^{1} d\cos\theta \int_{v_{\rm min}}^{v_{\rm max}} v f(v) F_{\rm DM}^2(q, v)\, dv, \quad (1)$$

where N_T is the number of target nucleus in the detector, $\rho_{\rm DM} = 0.3\ {\rm GeV\,cm^{-3}}$ is the local DM density, m_D is the DM mass. For the DM–nucleus differential scattering cross section $d\sigma_N/dE_R$, we have taken the following form [11]

$$\frac{d\sigma_N}{dE_R} = A^2 \frac{m_N \sigma_n}{2v^2 \mu_n^2} F_N^2(q) F_{\rm DM}^2(q, v), \quad (2)$$

where A is the mass number of target nucleus, σ_n is the DM–nucleon scattering cross section. In Eq. (2), we have required that the proton and neutron have the same contribution. The DM–nucleon reduced mass is given by $\mu_n = m_D m_n/(m_D + m_n)$ where m_n is the nucleon mass. The recoil energy E_R is related to the transferred momentum q and the target nucleus mass m_N through $q^2 = 2m_N E_R$. The DM velocity distribution function $f(v)$ in the galactic frame is usually assumed to be the Maxwell–Boltzmann distribution with velocity dispersion $v_0 = 220$ km/s, truncated at the galactic escape velocity $v_{\rm esc} = 544$ km/s. In the Earth's rest frame, we can derive

$$f(v) = \frac{1}{(\pi v_0^2)^{3/2}} e^{-(\vec{v}+\vec{v}_e)^2/v_0^2}, \quad (3)$$

where v is the DM velocity with respect to the Earth and $v_e \approx v_\odot = v_0 + 12$ km/s is the Earth's speed relative to the galactic halo. It is worthwhile to stress that the contribution of the Earth's orbit velocity to v_e has been neglected since we do not focus on the annual modulation. With the help of $|\vec{v} + \vec{v}_e| \leqslant v_{\rm esc}$, one can obtain the maximum DM velocity

$$v_{\rm max} = \sqrt{v_{\rm esc}^2 - v_e^2 + v_e^2 \cos\theta^2} - v_e \cos\theta, \quad (4)$$

where θ is the angle between $\vec{v}$ and $\vec{v}_e$. For a given recoil energy E_R, one can easily derive the minimum DM velocity

$$v_{\rm min} = \frac{\sqrt{2m_N E_R}}{2\mu_N}, \quad (5)$$

where $\mu_N = m_D m_N/(m_D + m_N)$ is the DM–nucleus reduced mass. For the nuclear form factor $F_N^2(q)$, we use the Helm form factor [16]

$$F_N^2(q) = \left(\frac{3j_1(qR_1)}{qR_1}\right)^2 e^{-q^2 s^2} \quad (6)$$

with $R_1 = \sqrt{c^2 + \frac{7}{3}\pi^2 a^2 - 5s^2}$ and $c \simeq 1.23A^{1/3} - 0.60$ fm [17]. Here we take $s \simeq 0.9$ fm and $a \simeq 0.52$ fm [17]. $j_1(x) = \sin x/x^2 - \cos x/x$ is a spherical Bessel function of the first kind. For the usual contact interaction, the DM form factor $F_{\rm DM}^2(q, v) = 1$ is independent of the transferred momentum q and the DM relative velocity v. In this paper, we shall focus on some momentum and velocity dependent DM form factors and discuss their effects on the DM direct detection cross section and the DM solar capture rate.

Table 1
The momentum and velocity dependent DM form factors for the heavy and light mediator mass scenarios with $V^2 = v^2 - q^2/(4\mu_N^2)$, $q_{\rm ref} = 100$ MeV and $V_{\rm ref} = v_0$.

Case	$\lvert\mathcal{M}\rvert^2$ $(m_\phi^2 \gg q^2)$	$F_{\rm DM}^2$ $(m_\phi^2 \gg q^2)$	Case	$\lvert\mathcal{M}\rvert^2$ $(m_\phi^2 \ll q^2)$	$F_{\rm DM}^2$ $(m_\phi^2 \ll q^2)$
1	$\lvert\mathcal{M}\rvert^2 \propto 1$	$F_{\rm DM}^2 = 1$	q^{-4}	$\lvert\mathcal{M}\rvert^2 \propto q^{-4}$	$F_{\rm DM}^2 = q_{\rm ref}^4/q^4$
q^2	$\lvert\mathcal{M}\rvert^2 \propto q^2$	$F_{\rm DM}^2 = q^2/q_{\rm ref}^2$	q^{-2}	$\lvert\mathcal{M}\rvert^2 \propto q^{-2}$	$F_{\rm DM}^2 = q_{\rm ref}^2/q^2$
V^2	$\lvert\mathcal{M}\rvert^2 \propto V^2$	$F_{\rm DM}^2 = V^2/V_{\rm ref}^2$	V^2q^{-4}	$\lvert\mathcal{M}\rvert^2 \propto V^2q^{-4}$	$F_{\rm DM}^2 = V^2q_{\rm ref}^4/(V_{\rm ref}^2q^4)$
q^4	$\lvert\mathcal{M}\rvert^2 \propto q^4$	$F_{\rm DM}^2 = q^4/q_{\rm ref}^4$	1	$\lvert\mathcal{M}\rvert^2 \propto 1$	$F_{\rm DM}^2 = 1$
V^4	$\lvert\mathcal{M}\rvert^2 \propto V^4$	$F_{\rm DM}^2 = V^4/V_{\rm ref}^4$	V^4q^{-4}	$\lvert\mathcal{M}\rvert^2 \propto V^4q^{-4}$	$F_{\rm DM}^2 = V^4q_{\rm ref}^4/(V_{\rm ref}^4q^4)$
V^2q^2	$\lvert\mathcal{M}\rvert^2 \propto V^2q^2$	$F_{\rm DM}^2 = V^2q^2/(V_{\rm ref}^2q_{\rm ref}^2)$	V^2q^{-2}	$\lvert\mathcal{M}\rvert^2 \propto V^2q^{-2}$	$F_{\rm DM}^2 = V^2q_{\rm ref}^2/(V_{\rm ref}^2q^2)$

2.2. Momentum and velocity dependent DM form factors

Usually, one can build some DM models and exactly calculate the DM direct detection cross section. On the other hand, the DM–nucleus interaction can be generally constructed from 16 model-independent operators in the non-relativistic (NR) limit [18,19]. Any other scalar operators involving at least one of the two spins can be expressed as a linear combination of the 16 independent operators with SI coefficients that may depend on q^2 and $\vec{V}^2 \equiv (\vec{v} - \vec{q}/(2\mu_N))^2 = v^2 - q^2/(4\mu_N^2)$. It is convenient for us to phenomenologically analyze the momentum and velocity dependent DM–nucleus interactions from these NR operators. Here we only focus on the following four SI NR operators in the momentum space [18,19]:

$$\begin{aligned}
&\mathcal{O}_1 = 1,\\
&\mathcal{O}_2 = i\vec{s}_D \cdot \vec{q},\\
&\mathcal{O}_3 = \vec{s}_D \cdot \vec{V},\\
&\mathcal{O}_4 = i\vec{s}_D \cdot (\vec{V} \times \vec{q}).
\end{aligned} \tag{7}$$

Considering the possible contributions of q^2 or V^2 in the coefficients, we phenomenologically discuss five kinds of momentum and velocity dependent DM form factors $F_{\rm DM}^2(q, v)$ up to q and $\vec{V}$ quartic terms in the amplitude squared $|\mathcal{M}|^2$. The five DM form factors and the usual contact interaction case have been listed in the third column of Table 1. Since the transferred momentum q in many direct detection experiments is order of 100 MeV, we take $q_{\rm ref} = 100$ MeV as the reference transferred momentum to normalize q. Similarly, we use $V_{\rm ref} = v_0$ to normalize $V = \sqrt{v^2 - \frac{q^2}{4\mu_N^2}}$. Here we have assumed that the mass m_ϕ of mediator between DM particles and quarks is far larger than the transferred momentum q, namely $m_\phi^2 \gg q^2$. If $m_\phi^2 \ll q^2$, $F_{\rm DM}^2(q, v)$ should contain the factor $1/q^4$ which comes from the squared propagator $(q^2 + m_\phi^2)^{-2}$. For the light mediator mass scenario, the corresponding 6 kinds of $F_{\rm DM}^2(q, v)$ cases have been listed in the sixth column of Table 1. In Section 4, we shall discuss the $m_\phi^2 \sim \mathcal{O}(q^2)$ scenario through varying m_ϕ.

2.3. New upper limits on σ_n

In this paper, we do not try to reconcile the tension between the DAMA annual modulation signal and other direct detection exclusions by use of the momentum and velocity dependent

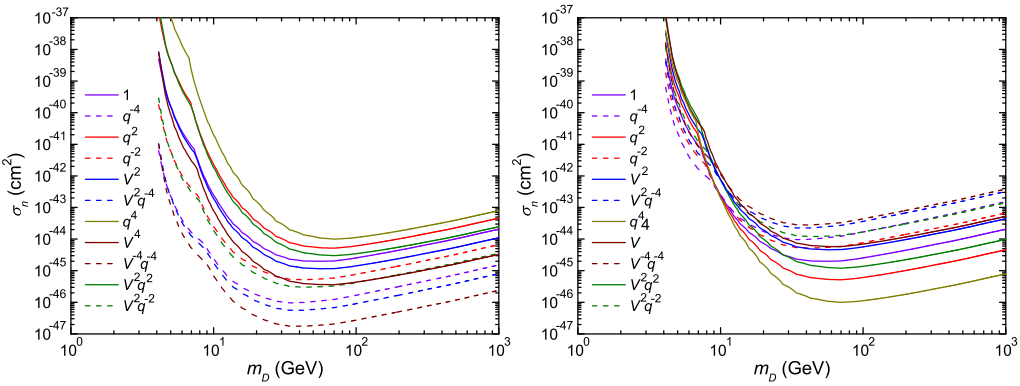

Fig. 1. The new upper limits on σ_n for different $F^2_{\rm DM}(q, v)$ with $q_{\rm ref} = 100$ MeV; $V_{\rm ref} = v_0$ (left panel) and $q_{\rm ref} = 10\sqrt{10}$ MeV; $V_{\rm ref} = 2v_0$ (right panel) from the XENON100 and XENON10.

DM–nucleus interactions. Here we only focus on the null observations and the corresponding upper limits on σ_n which are relevant to the maximal DM solar capture rate. Currently, the most stringent limit on σ_n comes from XENON100 [14] and XENON10 [15]. It should be mentioned that this limit is only valid for the usual contact interaction, namely $F^2_{\rm DM}(q, v) = 1$. For the momentum and velocity dependent $F^2_{\rm DM}(q, v)$, we should recalculate their limits from the reported results of XENON100 and XENON10.

The recoil energy window of the DM search region in the XENON100 is chosen between $3 \sim 30$ photoelectrons (PE), corresponding to $6.6\,{\rm keV} \leqslant E_R \leqslant 43.3\,{\rm keV}$. The relation of E_R and PE number S1 is given by [14]

$$\mathrm{S1}(E_R) = 3.73\,\mathrm{PE} \times E_R \times \mathcal{L}_{\rm eff}, \tag{8}$$

where $\mathcal{L}_{\rm eff}$ is the scintillation efficiency which has been measured above 3 keV. The $\mathcal{L}_{\rm eff}$ parametrization can be found in Ref. [20]. Here we assume that the produced PE number of a nucleus recoil event satisfies the Poissonian distribution and Eq. (8) denotes the mean value. In this case, the event with $E_R < 6.6$ keV will have a non-vanishing probability to generate a S1 signal above 3 PE. For the new lower threshold of E_R, we take $E_R \geqslant 3.0$ keV which can pass the ionization yield $S2$ cut [11,21].

The search recoil energy range of XENON10 is $1.4\,{\rm keV} \leqslant E_R \leqslant 10.0\,{\rm keV}$ [15]. For $4\,{\rm GeV} \lesssim m_D \leqslant 20\,{\rm GeV}$, one can always find some parameter space among $1.4\,{\rm keV} \leqslant E_R \leqslant 10.0\,{\rm keV}$ to satisfy $v_{\rm min} < v_{\rm max}$. Therefore, we directly input $1.4\,{\rm keV} \leqslant E_R \leqslant 10.0\,{\rm keV}$ into Eq. (1) for the XENON10 analysis. Note that the upper limit with $v_0 = 230$ km/s and $v_{\rm esc} = 600$ km/s in Ref. [15] has been replaced by the corresponding limit with $v_0 = 220$ km/s and $v_{\rm esc} = 544$ km/s in the following parts.

Requiring the same event rate R for different $F^2_{\rm DM}(q, v)$, we deduce new bounds about σ_n for each $F^2_{\rm DM}(q, v)$ from the $F^2_{\rm DM}(q, v) = 1$ case (the reported limits of XENON100 and XENON10). Our numerical results have been shown in the left panel of Fig. 1. The same color solid and dashed lines describe the heavy and the corresponding light mediator mass scenarios, respectively. In Fig. 1, the number 1 denotes the $F^2_{\rm DM}(q, v) = 1$ case, V^2q^{-2} denotes the $F^2_{\rm DM}(q, v) = V^2q^2_{\rm ref}/(V^2_{\rm ref}q^2)$ case, and so on. It is meaningless for us to compare different lines since these limits are dependent on $q_{\rm ref}$ and $V_{\rm ref}$. For illustration, we plot our numerical results with $q_{\rm ref} = 10\sqrt{10}\,{\rm MeV}$ and $V_{\rm ref} = 2v_0$ in the right panel of Fig. 1. Some kinks

around $m_D = 8$ GeV arise from the different slopes of the predicted limits of XENON100 and XENON10. It is should be mentioned that the new upper bound from the XENON100 and XENON10 is still the most stringent limit for each $F^2_{\rm DM}(q, v)$ when we recalculate other experimental results [22].

3. Dark matter solar capture

When the halo DM particles elastically scatter with nuclei in the Sun, they may lose most of their energy and are trapped by the Sun [1]. On the other hand, the DM annihilation in the Sun depletes the DM population. The evolution of the DM number N in the Sun is given by the following equation [23]:

$$\dot{N} = C_\odot - C_A N^2, \tag{9}$$

where the dot denotes differentiation with respect to time. The DM solar capture rate $C_\odot$ in Eq. (9) is proportional to the DM–nucleon scattering cross section σ_n. In the next subsection, we shall give the exact formulas to calculate $C_\odot$. The last term $C_A N^2$ in Eq. (9) controls the DM annihilation rate in the Sun. The coefficient C_A depends on the thermal-average of the annihilation cross section times the relative velocity $\langle \sigma v \rangle$ and the DM distribution in the Sun. To a good approximation, one can obtain $C_A = \langle \sigma v \rangle / V_{\rm eff}$, where $V_{\rm eff} = 5.8 \times 10^{30}\ {\rm cm}^3\ (1\ {\rm GeV}/m_D)^{3/2}$ is the effective volume of the core of the Sun [23,24]. In Eq. (9), we have neglected the evaporation effect since this effect is very small when $m_D \gtrsim 4$ GeV [25,26]. One can easily solve the evolution equation and derive the DM solar annihilation rate [23]

$$\Gamma_A = \frac{1}{2} C_\odot \tanh^2(t_\odot \sqrt{C_\odot C_A}), \tag{10}$$

where $t_\odot \simeq 4.5$ Gyr is the age of the solar system. If $t_\odot \sqrt{C_\odot C_A} \gg 1$, the DM annihilation rate reaches equilibrium with the DM capture rate. In this case, we derive the maximal DM annihilation rate $\Gamma_A = C_\odot/2$. It is clear that the DM annihilation signals from the Sun are entirely determined by $C_\odot$.

3.1. DM solar capture rate and annihilation rate

By use of the DM angular momentum conservation in the solar gravitational field, one can obtain the following DM capture rate $C_\odot$ [24]:

$$C_\odot = \sum_{N_i} \int 4\pi r^2\, dr \int \frac{f(u)}{u} \omega \Omega_{N_i}(\omega)\, d^3u \tag{11}$$

with

$$f(u) = \frac{1}{(\pi v_0^2)^{3/2}} e^{-(\vec{u}+\vec{v}_\odot)^2/v_0^2}, \tag{12}$$

where $f(u)$ is the DM velocity distribution, u is the DM velocity at infinity with respect to the Sun's rest frame, $v_\odot = v_0 + 12$ km/s is the Sun's speed relative to the galactic halo. $\Omega_{N_i}(\omega)$ is the rate per unit time at which a DM particle with the incident velocity ω scatters to an orbit within the Jupiter's orbit. $\Omega_{N_i}(\omega)$ is given by

$$\Omega_{N_i}(\omega) = n_{N_i}(r) \sigma_{N_i}(\omega) \omega \rho_{\rm DM}/m_D, \tag{13}$$

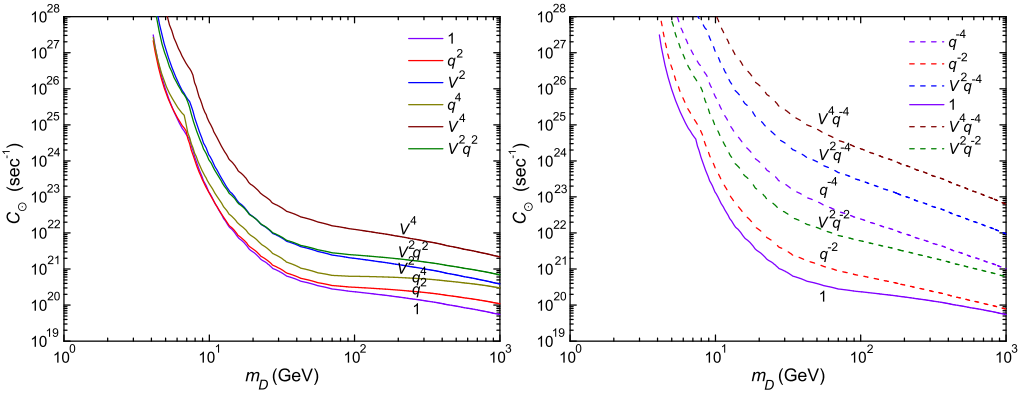

Fig. 2. The predicted maximal DM solar capture rates $C_\odot$ for the heavy (left panel) and light (right panel) mediator mass scenarios.

where $n_{N_i}(r)$ and $\omega(r) = \sqrt{u^2 + v_{\rm esc}^2(r)}$ are the number density of element N_i and the DM incident velocity at radius r inside the Sun, respectively. The escape velocity $v_{\rm esc}(r)$ from the Sun at the radius r can be approximately written as $v_{\rm esc}^2(r) = v_c^2 - (v_c^2 - v_s^2)M(r)/M_\odot$ [27], where $v_c = 1354$ km/s and $v_s = 795$ km/s are the escape velocity at the Sun's center and surface, respectively. $M_\odot = 1.989 \times 10^{33}$ g is the solar mass and $M(r)$ is the mass within the radius r. $\sigma_{N_i}(\omega)$ in Eq. (13) is the scattering cross section between a stationary target nucleus N_i in the Sun and an incident DM particle with velocity ω. The non-relativistic effective theory allows us to express $\sigma_{N_i}(\omega)$ as

$$\sigma_{N_i}(\omega) = \frac{A_i^2 \sigma_n}{2\omega^2 \mu_n^2} \int_{q_{\rm min}}^{2\mu_{N_i}\omega} F_{N_i}^2(q) F_{\rm DM}^2(q,\omega) q\, dq, \tag{14}$$

where $q_{\rm min} = \sqrt{m_D m_{N_i}[u^2 + v_{\rm esc}^2(r = 5.2{\rm AU})]}$ is the minimum transferred momentum needed for capture and $v_{\rm esc}(r = 5.2{\rm AU}) = 18.5$ km/s denotes the DM escape velocity from the Sun at the Jupiter's orbit [8,28].

In our calculation, we sum over the following elements in the Sun: ^{1}H, ^{4}He, ^{12}C, ^{14}N, ^{16}O, ^{17}O, Ne, Mg, Si, S and Fe. The number densities $n_{N_i}(r)$ of these elements and $M(r)$ can be obtained from the calculation of the standard solar model (SSM). Here we employ the SSM GS98 [29] to calculate the DM solar capture rate $C_\odot$ in Eq. (11) with the help of σ_n in the left panel of Fig. 1. Our numerical results have been shown in Fig. 2. We find that for almost whole of the m_D parameter space the predicted $C_\odot$ from the standard contact interaction is smaller than those from the momentum and velocity dependent DM form factor cases. This means that the momentum and velocity dependent DM form factor cases can give larger DM annihilation signals than that from the usual contact interaction case. The same color solid and dashed lines in Fig. 2 describe the heavy and the corresponding light mediator mass scenarios, respectively. The light mediator mass scenario can usually produce the larger $C_\odot$ than the corresponding heavy mediator mass scenario. However one can derive the opposite conclusion for the q^4 and 1 cases. It should be mentioned that our numerical results in Fig. 2 are independent of $q_{\rm ref}$ and $V_{\rm ref}$.

3.2. Constraints from the Super-Kamiokande and IceCube

Due to the interactions of the DM annihilation products in the Sun, only the neutrino can escape from the Sun and reach the Earth. For the given DM mass and DM annihilation channel α, the differential muon neutrino flux at the surface of the Earth from per DM pair annihilation in the Sun can be written as

$$\frac{d\Phi^{\alpha}_{\nu_\mu}}{dE_{\nu_\mu}} = \frac{\Gamma_A}{4\pi R^2_{\rm ES}} \frac{dN^{\alpha}_{\nu_\mu}}{dE_{\nu_\mu}}, \tag{15}$$

where $R_{\rm ES} = 1.496 \times 10^{13}$ cm is the Earth–Sun distance. $dN^{\alpha}_{\nu_\mu}/dE_{\nu_\mu}$ denotes the energy distribution of neutrinos at the surface of the Earth produced by the final state α through hadronization and decay processes in the core of the Sun. It should be mentioned that some produced particles, such as the muon and abundantly produced light hadrons can lose almost total energy before they decay due to their interactions in the Sun. In addition, we should consider the neutrino interactions in the Sun and neutrino oscillations. In this paper, we use the program package WimpSim [30] to calculate $dN^{\alpha}_{\nu_\mu}/dE_{\nu_\mu}$ with the following neutrino oscillation parameters [31,32]:

$$\begin{aligned} &\sin^2\theta_{12} = 0.32, \qquad \sin^2\theta_{23} = 0.49, \qquad \sin^2\theta_{13} = 0.026, \qquad \delta = 0.83\pi, \\ &\Delta m^2_{21} = 7.62 \times 10^{-5}\ \text{eV}^2, \qquad \Delta m^2_{31} = 2.53 \times 10^{-3}\ \text{eV}^2. \end{aligned} \tag{16}$$

In addition, we should also calculate the differential muon anti-neutrino flux which can be evaluated by an equation similar to Eq. (15).

These high energy neutrinos interact with the Earth rock or ice to produce upgoing muons which may be detected by the water Cherenkov detector Super-Kamiokande [4] and the neutrino telescope IceCube [5,6]. Due to the produced muons scattered from the primary neutrino direction and the multiple Coulomb scattering of muons on route to the detector, the final directions of muons are spread. For 10 GeV $\leqslant m_D \leqslant$ 1000 GeV, the cone half-angle which contains more than 90% of the expected event numbers ranges from 6° to 30° for the Super-Kamiokande when we assume the $b\bar{b}$ annihilation channel. The cone half-angles will be smaller for the other DM annihilation channels considered in this paper with the same DM mass. In terms of the results of cone half-angle θ in Tables 1 and 2 of Ref. [4], we conservatively take some reasonable θ for other DM annihilation channels and several representative DM masses as shown in Table 2.

The neutrino induced upgoing muon events in the Super-Kamiokande can be divided into three categories: stopping, non-showering through-going and showering through-going [4]. The fraction of each upgoing muon category as a function of parent neutrino energy E_{ν_μ} has been shown in Fig. 2 of Ref. [4]. Then we use $dN^{\alpha}_{\nu_\mu}/dE_{\nu_\mu}$ to calculate the fraction of each category F^i as listed in Table 2. Once F^i is obtained, the 90% confidence level (CL) upper Poissonian limit N_{90} can be derived through the following formulas [4]:

$$90\% = \frac{\int_{\nu_s=0}^{N_{90}} L(n^i_{\rm obs}|\nu_s)\, d\nu_s}{\int_{\nu_s=0}^{\infty} L(n^i_{\rm obs}|\nu_s)\, d\nu_s} \tag{17}$$

and

$$L\big(n^i_{\rm obs}\big|\nu_s\big) = \prod_{i=1}^{3} \frac{(\nu_s F^i + n^i_{\rm BG})^{n^i_{\rm obs}}}{n^i_{\rm obs}!} e^{-(\nu_s F^i + n^i_{\rm BG})}, \tag{18}$$

Table 2
The relevant parameter summary to calculate the Super-Kamiokande constraints on Γ_A for different DM annihilation channels and masses. The units of m_D and ϕ_μ are GeV and 10^{-15} cm^{-2} s^{-1}.

Channel	m_D	θ	F^i (%)	N_{90}	ϕ_μ	Γ_A (s^{-1})	Channel	m_D	θ	F^i (%)	N_{90}	ϕ_μ	Γ_A (s^{-1})
$\nu_e\bar{\nu}_e$	4	30°	93.1; 5.5; 1.4	15.65	9.4	7.2×10^{24}	$\nu_\mu\bar{\nu}_\mu$	4	30°	93.1; 5.5; 1.4	15.65	9.4	6.7×10^{24}
$\nu_e\bar{\nu}_e$	6	30°	87.0; 9.9; 3.1	16.62	10.0	2.7×10^{24}	$\nu_\mu\bar{\nu}_\mu$	6	30°	87.0; 9.9; 3.1	16.62	10.0	2.4×10^{24}
$\nu_e\bar{\nu}_e$	10	30°	73.4; 19.3; 7.3	19.14	11.5	8.3×10^{23}	$\nu_\mu\bar{\nu}_\mu$	10	30°	73.4; 19.3; 7.3	19.14	11.5	6.7×10^{23}
$\nu_e\bar{\nu}_e$	10^2	7°	15.3; 58.6; 26.1	7.33	4.4	6.3×10^{21}	$\nu_\mu\bar{\nu}_\mu$	10^2	7°	17.8; 56.9; 25.3	7.35	4.4	1.9×10^{21}
$\nu_e\bar{\nu}_e$	10^3	3°	14.4; 53.6; 32.0	4.64	2.8	1.5×10^{21}	$\nu_\mu\bar{\nu}_\mu$	10^3	3°	17.4; 52.2; 30.4	4.60	2.8	9.6×10^{20}
$\nu_\tau\bar{\nu}_\tau$	4	30°	93.1; 5.5; 1.4	15.65	9.4	6.7×10^{24}	$\tau^+\tau^-$	4	30°	96.1; 3.2; 0.7	15.22	9.1	1.1×10^{26}
$\nu_\tau\bar{\nu}_\tau$	6	30°	87.0; 9.9; 3.1	16.62	10.0	2.4×10^{24}	$\tau^+\tau^-$	6	30°	94.9; 4.1; 1.0	15.40	9.2	2.0×10^{25}
$\nu_\tau\bar{\nu}_\tau$	10	30°	73.4; 19.3; 7.3	19.14	11.5	6.7×10^{23}	$\tau^+\tau^-$	10	30°	91.3; 6.7; 2.0	15.94	9.5	4.4×10^{24}
$\nu_\tau\bar{\nu}_\tau$	10^2	7°	20.8; 54.9; 24.3	7.35	4.4	3.0×10^{21}	$\tau^+\tau^-$	10^2	7°	44.8; 39.2; 16.0	6.81	4.1	1.4×10^{22}
$\nu_\tau\bar{\nu}_\tau$	10^3	3°	28.6; 48.2; 23.2	4.42	2.6	4.9×10^{20}	$\tau^+\tau^-$	10^3	3°	27.9; 48.8; 23.3	4.43	2.7	5.8×10^{20}
W^+W^-	81	8°	44.6; 39.4; 16.0	8.38	5.0	6.2×10^{22}	ZZ	92	8°	47.4; 37.4; 15.2	8.20	4.9	4.0×10^{22}
W^+W^-	10^2	7°	43.4; 40.1; 16.5	6.86	4.1	3.3×10^{22}	ZZ	10^2	7°	46.6; 37.9; 15.5	6.74	4.0	2.8×10^{22}
W^+W^-	10^3	3°	34.4; 44.6; 21.0	4.31	2.6	1.9×10^{21}	ZZ	10^3	3°	40.6; 40.6; 18.8	4.18	2.5	1.7×10^{21}
$b\bar{b}$	6	30°	96.7; 2.7; 0.6	15.14	9.1	1.5×10^{27}							
$b\bar{b}$	10	30°	95.6; 3.6; 0.8	15.29	9.2	1.3×10^{26}							
$b\bar{b}$	10^2	10°	77.2; 16.6; 6.2	10.93	6.5	5.9×10^{23}	$t\bar{t}$	175	10°	61.2; 27.7; 11.1	12.26	7.3	4.4×10^{22}
$b\bar{b}$	10^3	6°	58.6; 29.4; 12.0	6.43	3.9	2.4×10^{22}	$t\bar{t}$	10^3	6°	53.4; 32.5; 14.1	6.60	4.0	3.6×10^{21}

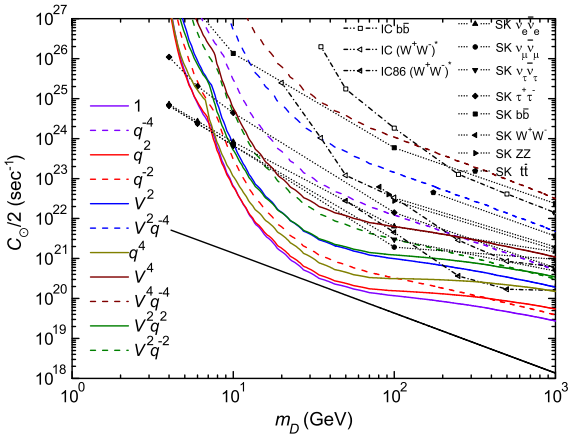

Fig. 3. The current Super-Kamiokande and IceCube constraints on $C_\odot/2$ with the assumption $\Gamma_A = C_\odot/2$ and the predicted maximal DM solar capture rates $C_\odot/2$ from Fig. 2 for different $F^2_{\rm DM}(q, v)$. The black solid line describes the equilibrium condition for $\langle\sigma v\rangle \approx 3.0 \times 10^{-26}\ {\rm cm}^3\ {\rm s}^{-1}$.

where ν_s is the expected real signal. The number of observed events of each category $n^i_{\rm obs}$ and the expected background of each category $n^i_{\rm BG}$ for different DM masses and cone half-angles can be found in Tables 1 and 2 of Ref. [4]. With the help of Eqs. (17) and (18), we estimate the 90% CL upper Poissonian limit on the number of upgoing muon events N_{90} and the corresponding 90% CL upper Poissonian limit of upgoing muon flux $\phi_\mu = N_{90}/(1.67 \times 10^{15}\ {\rm cm}^2\ {\rm s})$ as shown in Table 2.

With the help of Eq. (26) in Ref. [33], we numerically calculate the neutrino induced muon flux from per DM pair annihilation in the Sun. Then we directly derive the Super-Kamiokande constraints on Γ_A from the ϕ_μ values as listed in Table 2. In Fig. 3, we plot these results with the dotted lines and the predicted maximal DM solar capture rates $C_\odot/2$ from Fig. 2 for different $F^2_{\rm DM}(q, v)$. It should be mentioned that $\Gamma_A = C_\odot/2$ has been assumed in Fig. 3. As shown in Eq. (10), the assumption $\Gamma_A = C_\odot/2$ holds if $t_\odot\sqrt{C_\odot C_A} \gg 1$. For the usual s-wave thermally averaged annihilation cross section $\langle\sigma v\rangle \approx 3.0 \times 10^{-26}\ {\rm cm}^3\ {\rm s}^{-1}$ deduced from the DM relic density, we find that $t_\odot\sqrt{C_\odot C_A} \geqslant 3.0$ (namely $\tanh^2[t_\odot\sqrt{C_\odot C_A}] \geqslant 0.99$) requires $C_\odot/2 \geqslant 4.3 \times 10^{22}/(m_D/1\ {\rm GeV})^{3/2}\ {\rm s}^{-1}$ which has been plotted in Fig. 3 with the black solid line. Therefore the predicted $C_\odot/2$ above this line in Fig. 3 will satisfy the assumption $\Gamma_A = C_\odot/2$ when $\langle\sigma v\rangle \gtrsim 3.0 \times 10^{-26}\ {\rm cm}^3\ {\rm s}^{-1}$. In addition to the Super-Kamiokande experiment, the IceCube collaboration has also reported the upper limits on the DM annihilation rate Γ_A for the $\bar{b}b$ and W^+W^- ($\tau^+\tau^-$ below $m_D = 80.4$ GeV) channels in Table I of Ref. [5]. We plot these results with the dash-dotted lines in Fig. 3. The IC86$(W^+W^-)^*$ line shows the expected 180 days sensitivity of the completed IceCube detector [6]. Recently, the ANTARES neutrino telescope [7] has reported the first results which are comparable with those obtained by the Super-Kamiokande [4] and IceCube [5,6]. It is shown that the upper limits on $C_\odot$ (σ_n) from the Super-Kamiokande and IceCube are weaker than those from the current direct detection experiments for the usual SI DM–nucleus interaction. However, our numerical results in Fig. 3 clearly show the Super-Kamiokande and IceCube may give more stringent constraints than the XENON100 experiment for several momentum and velocity dependent DM–nucleus interactions with $m_D \gtrsim 10$ GeV and the assumption $\Gamma_A = C_\odot/2$.

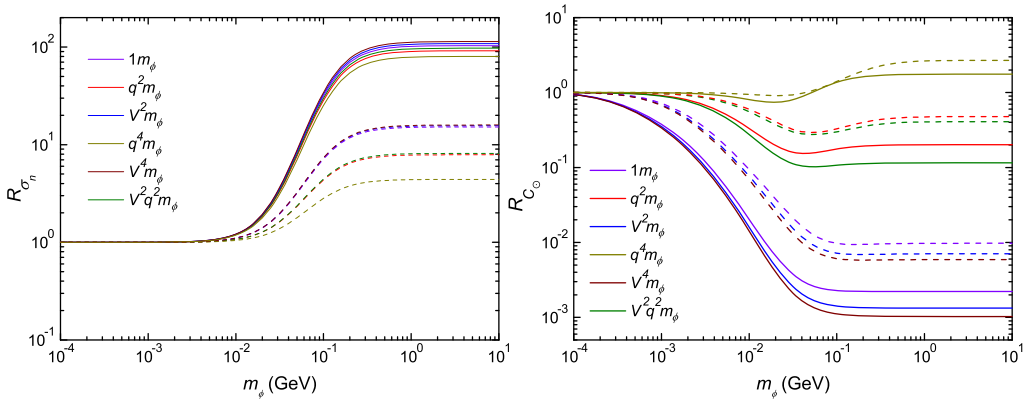

Fig. 4. The predicted σ_n and $C_\odot$ as a function of m_ϕ for $m_D = 10$ GeV and $m_D = 100$ GeV. The parameters R_{σ_n} and $R_{C_\odot}$ are defined as $R_{\sigma_n} \equiv \sigma_n/\sigma_n(m_\phi^2 \ll q^2, q_{\rm ref}^2)$ and $R_{C_\odot} \equiv C_\odot/C_\odot(m_\phi^2 \ll q^2, q_{\rm ref}^2)$. The solid and dashed lines describe $m_D = 10$ GeV and $m_D = 100$ GeV cases, respectively.

In Fig. 3, one may find that the Super-Kamiokande experiment can significantly constrain the low mass DM for all DM form factors in Table 1 when the DM particles dominantly annihilate into neutrino pairs or $\tau^+\tau^-$. If $m_D \gtrsim 20$ GeV, both Super-Kamiokande and IceCube cannot constrain any momentum and velocity dependent case except for the V^4q^{-4} case, when the annihilation channel is the $b\bar{b}$, and the $1, q^2, q^{-2}, q^4, V^2, V^2q^2$ and V^2q^{-2} cases for any annihilation channel. The V^4q^{-4} and V^2q^{-4} cases can be significantly constrained by the above two experiments if the DM annihilation final states are neutrinos, tau leptons or gauge bosons. For the W^+W^- channel, the IceCube gives the stronger constraint than the Super-Kamiokande when $m_D \gtrsim 100$ GeV. The future IceCube result IC86$(W^+W^-)^*$ has ability to constrain the q^{-4}, V^2, V^4, V^2q^2 and V^2q^{-2} cases with $m_D \gtrsim 200$ GeV. Since $C_\odot$ is proportional to σ_n, the upper limits on $C_\odot$ in Fig. 3 will move downward if σ_n in Fig. 1 becomes smaller. The Super-Kamiokande experiment can still constrain the momentum and velocity dependent DM–nucleus interactions for the low DM mass region even if σ_n is reduced by 2 orders.

4. The mediator mass m_ϕ effect on σ_n and $C_\odot$

In Section 2.2, we have taken two extreme scenarios for the mediator mass m_ϕ: $m_\phi^2 \gg q^2$ and $m_\phi^2 \ll q^2$. Here we shall consider the $m_\phi^2 \sim \mathcal{O}(q^2)$ scenario and discuss the m_ϕ effect on σ_n and $C_\odot$. In this case, the momentum and velocity dependent DM form factors are relevant to m_ϕ. It is found that the m_ϕ dependent DM form factors $F_{\rm DM}^2(q, v, m_\phi)$ can be written by the product of the third column of Table 1 and a factor $(q_{\rm ref}^2 + m_\phi^2)^2/(q^2 + m_\phi^2)^2$. The two DM form factors in each row of Table 1 are two extreme cases of the m_ϕ dependent DM form factor $F_{\rm DM}^2(q, v, m_\phi)$. For example, one can easily obtain $F_{\rm DM}^2(q, v) = q^2/q_{\rm ref}^2$ with $m_\phi^2 \gg q^2, q_{\rm ref}^2$ and $F_{\rm DM}^2(q, v) = q_{\rm ref}^2/q^2$ with $m_\phi^2 \ll q^2, q_{\rm ref}^2$ from $F_{\rm DM}^2(q, v, m_\phi) = (q^2/q_{\rm ref}^2)(q_{\rm ref}^2 + m_\phi^2)^2/(q^2 + m_\phi^2)^2$. Therefore, we have 6 kinds of m_ϕ dependent DM form factors $F_{\rm DM}^2(q, v, m_\phi)$. Here we use $1m_\phi, q^2m_\phi, V^2m_\phi, q^4m_\phi, V^4m_\phi$ and $V^2q^2m_\phi$ to express them.

Using the above 6 m_ϕ dependent DM form factors, we calculate σ_n and $C_\odot$ for two representative DM masses: $m_D = 10$ GeV and $m_D = 100$ GeV. Our numerical results have been shown in Fig. 4. The parameters R_{σ_n} and $R_{C_\odot}$ in Fig. 4 are defined as $R_{\sigma_n} \equiv \sigma_n/\sigma_n(m_\phi^2 \ll q^2, q_{\rm ref}^2)$

and $R_{C_\odot} \equiv C_\odot/C_\odot(m_\phi^2 \ll q^2, q_{\rm ref}^2)$. $\sigma_n(m_\phi^2 \ll q^2, q_{\rm ref}^2)$ and $C_\odot(m_\phi^2 \ll q^2, q_{\rm ref}^2)$ denote the DM scattering cross section and solar capture rate in the $m_\phi^2 \ll q^2, q_{\rm ref}^2$ case, respectively. One may see from Fig. 4 (left panel) that σ_n will remarkably increase as m_ϕ increases when $m_\phi \sim q_{\rm ref} = 0.1$ GeV. For $m_\phi \lesssim 0.01$ GeV and $m_\phi \gtrsim 0.2$ GeV, the predicted σ_n is insensitive to m_ϕ. These features can be easily understood from the forms of $F_{\rm DM}^2(q, v, m_\phi)$. For the light DM mass $m_D = 10$ GeV, our numerical results show that 6 kinds of m_ϕ dependent DM form factors can produce the similar curves. As shown in Fig. 4 (right panel), the predicted $C_\odot$ approaches to a constant as well as σ_n if $m_\phi \gtrsim 0.2$ GeV. For $m_\phi < 0.2$ GeV, $C_\odot$ can usually decrease as m_ϕ increases. We find that the $q^2 m_\phi$, $q^4 m_\phi$ and $V^2 q^2 m_\phi$ cases have the minimums around $m_\phi \approx 0.04$ GeV for $C_\odot$. In fact, the DM solar capture rates with a fixed σ_n in the $q^2 m_\phi$, $q^4 m_\phi$ and $V^2 q^2 m_\phi$ cases are the monotone decreasing functions of m_ϕ. Therefore the minimums arise from the monotone increasing σ_n. When the σ_n increase is larger than the $C_\odot$ (with a fixed σ_n) decrease, we can derive $R_{C_\odot} > 1$, just like the $q^4 m_\phi$ case in the right panel of Fig. 4. In terms of the results in Fig. 4, the DM solar capture rate in the m_ϕ dependent scenario will quickly move from the dashed line to the corresponding color solid line as m_ϕ increases in Fig. 3. When $m_\phi \gtrsim 0.2$ GeV, the m_ϕ dependent scenario will approach to the heavy mediator mass scenario.

5. Discussions and conclusions

So far, we have used the usual Helm nuclear form factor for $F_N^2(q)$ in Eqs. (1) and (14) to calculate σ_n and $C_\odot$. In fact, the exact $F_N^2(q)$ contains the standard SI nuclear form factor (Helm nuclear form factor) and an important correction from the angular-momentum of unpaired nucleons within the nucleus for the NR operators $\mathcal{O}_3$ and $\mathcal{O}_4$ in Eq. (7) [19]. The correction is comparable with the standard SI nuclear form factor for nuclei with unpaired protons and neutrons when $m_D \gtrsim m_N$. By use of the relevant formulas in Appendix A of Ref. [19], we numerically calculate this correction contribution to the XENON100 and XENON10 experiments and find that it is smaller than 10% and can be neglected for our analysis about σ_n. In the previous sections, the predicted $C_\odot$ arises from the contributions of ^{1}H, ^{4}He, ^{12}C, ^{14}N, ^{16}O, Ne, Mg, Si, S and Fe. Since these elements or dominant isotopes have not the unpaired protons and neutrons within the nucleus, our numerical results about $C_\odot$ are not significantly changed.

In conclusion, we have investigated the SI momentum and velocity dependent DM–nucleus interactions and discussed their effects on σ_n and $C_\odot$. In terms of the NR effective theory, we phenomenologically discuss 10 kinds of momentum and velocity dependent DM form factors $F_{\rm DM}^2(q, v)$. Using these DM form factors, we have recalculated the corresponding upper limits on σ_n from the XENON100 and XENON10 experimental results. Each upper limit on σ_n can be used to calculate the corresponding maximal DM solar capture rate $C_\odot$. Our numerical results have shown that the momentum and velocity dependent DM form factor cases can give larger DM annihilation signals than the usual contact interaction case for almost the whole parameter space. The light mediator mass scenario can usually produce the larger $C_\odot$ than the corresponding heavy mediator mass scenario except for the q^4 and 1 cases. On the other hand, we have also deduced the Super-Kamiokande's constraints on $C_\odot/2$ for 8 typical DM annihilation channels with the equilibrium assumption $\Gamma_A = C_\odot/2$. In contrast to the usual contact interaction, the Super-Kamiokande and IceCube experiments can give more stringent limits on σ_n than the latest XENON100 experiment for several momentum and velocity dependent DM form factors when $m_D \gtrsim 10$ GeV and $\Gamma_A = C_\odot/2$. In addition, we have also considered 6 kinds of m_ϕ dependent DM form factors and analyzed their effects on σ_n and $C_\odot$. We find that $C_\odot$ will quickly move from the light mediator mass scenario to the corresponding heavy mediator mass scenario as m_ϕ

increases. When $m_\phi \gtrsim 0.2$ GeV, the m_ϕ dependent scenario will approach to the corresponding heavy mediator mass scenario.

Acknowledgements

This work is supported in part by the National Basic Research Program of China (973 Program) under Grants No. 2010CB833000; the National Nature Science Foundation of China (NSFC) under Grants No. 10821504 and No. 10905084; and the Project of Knowledge Innovation Program (PKIP) of the Chinese Academy of Science.

References

[1] For a review on dark matter and its particle interpretation, see G. Jungman, M. Kamionkowski, K. Griest, Phys. Rep. 267 (1996) 195.
[2] For a review on dark matter and its particle interpretation, see G. Bertone, D. Hooper, J. Silk, Phys. Rep. 405 (2005) 279.
[3] P.A.R. Ade, et al., Planck Collaboration, arXiv:1303.5076 [astro-ph.CO].
[4] T. Tanaka, et al., Super-Kamiokande Collaboration, Astrophys. J. 742 (2011) 78, arXiv:1108.3384 [astro-ph.HE].
[5] M. Aartsen, et al., IceCube Collaboration, arXiv:1212.4097 [astro-ph.HE].
[6] R. Abbasi, et al., IceCube Collaboration, Phys. Rev. D 85 (2012) 042002, arXiv:1112.1840 [astro-ph.HE].
[7] S. Adrian-Martinez, et al., ANTARES Collaboration, arXiv:1302.6516 [astro-ph.HE].
[8] J. Kumar, J.G. Learned, S. Smith, K. Richardson, Phys. Rev. D 86 (2012) 073002, arXiv:1204.5120 [hep-ph].
[9] R. Foot, Phys. Lett. B 703 (2011) 7, arXiv:1106.2688 [hep-ph];
R. Foot, Phys. Rev. D 86 (2012) 023524, arXiv:1203.2387 [hep-ph];
T. Schwetz, J. Zupan, J. Cosmol. Astropart. Phys. 1108 (2011) 008, arXiv:1106.6241 [hep-ph];
N. Fornengo, P. Panci, M. Regis, Phys. Rev. D 84 (2011) 115002, arXiv:1108.4661 [hep-ph].
[10] S. Chang, A. Pierce, N. Weiner, J. Cosmol. Astropart. Phys. 1001 (2010) 006, arXiv:0908.3192 [hep-ph].
[11] M. Farina, D. Pappadopulo, A. Strumia, T. Volansky, J. Cosmol. Astropart. Phys. 1111 (2011) 010, arXiv:1107.0715 [hep-ph].
[12] A.L. Fitzpatrick, W. Haxton, E. Katz, N. Lubbers, Y. Xu, arXiv:1211.2818 [hep-ph].
[13] E. Masso, S. Mohanty, S. Rao, Phys. Rev. D 80 (2009) 036009, arXiv:0906.1979 [hep-ph];
S. Chang, N. Weiner, I. Yavin, Phys. Rev. D 82 (2010) 125011, arXiv:1007.4200 [hep-ph];
V. Barger, W.-Y. Keung, D. Marfatia, Phys. Lett. B 696 (2011) 74, arXiv:1007.4345 [hep-ph];
A.L. Fitzpatrick, K.M. Zurek, Phys. Rev. D 82 (2010) 075004, arXiv:1007.5325 [hep-ph];
T. Banks, J.-F. Fortin, S. Thomas, arXiv:1007.5515 [hep-ph];
E. Del Nobile, C. Kouvaris, P. Panci, F. Sannino, J. Virkajarvi, J. Cosmol. Astropart. Phys. 1208 (2012) 010, arXiv:1203.6652 [hep-ph].
[14] E. Aprile, et al., XENON100 Collaboration, Phys. Rev. Lett. 109 (2012) 181301, arXiv:1207.5988 [astro-ph.CO].
[15] J. Angle, et al., XENON10 Collaboration, Phys. Rev. Lett. 107 (2011) 051301, arXiv:1104.3088 [astro-ph.CO].
[16] R.H. Helm, Phys. Rev. 104 (1956) 1466.
[17] J.D. Lewin, P.F. Smith, Astropart. Phys. 6 (1996) 87.
[18] J. Fan, M. Reece, L.-T. Wang, J. Cosmol. Astropart. Phys. 1011 (2010) 042, arXiv:1008.1591 [hep-ph].
[19] A.L. Fitzpatrick, W. Haxton, E. Katz, N. Lubbers, Y. Xu, J. Cosmol. Astropart. Phys. 1302 (2013) 004, arXiv:1203.3542 [hep-ph].
[20] E. Aprile, et al., XENON100 Collaboration, Phys. Rev. Lett. 107 (2011) 131302, arXiv:1104.2549 [astro-ph.CO].
[21] C. Savage, G. Gelmini, P. Gondolo, K. Freese, Phys. Rev. D 83 (2011) 055002, arXiv:1006.0972 [astro-ph.CO].
[22] Z. Ahmed, et al., CDMS-II Collaboration, Science 327 (2010) 1619, arXiv:0912.3592 [astro-ph.CO];
Z. Ahmed, et al., CDMS-II Collaboration, Phys. Rev. Lett. 106 (2011) 131302, arXiv:1011.2482 [astro-ph.CO];
E. Armengaud, et al., EDELWEISS Collaboration, Phys. Lett. B 702 (2011) 329, arXiv:1103.4070 [astro-ph.CO];
E. Armengaud, et al., EDELWEISS Collaboration, Phys. Rev. D 86 (2012) 051701, arXiv:1207.1815 [astro-ph.CO];
M. Felizardo, et al., SIMPLE, Phys. Rev. Lett. 108 (2012) 201302, arXiv:1106.3014 [astro-ph.CO];
D.Y. Akimov, et al., ZEPLIN-III, Phys. Lett. B 709 (2012) 14, arXiv:1110.4769 [astro-ph.CO].
[23] K. Griest, D. Seckel, Nucl. Phys. B 283 (1987) 681;
K. Griest, D. Seckel, Nucl. Phys. B 296 (1988) 1034 (Erratum).

[24] A. Gould, Astrophys. J. 321 (1987) 571.
[25] A. Gould, Astrophys. J. 321 (1987) 560.
[26] D. Hooper, F. Petriello, K.M. Zurek, M. Kamionkowski, Phys. Rev. D 79 (2009) 015010, arXiv:0808.2464 [hep-ph].
[27] A. Gould, Astrophys. J. 388 (1992) 338.
[28] A.H.G. Peter, Phys. Rev. D 79 (2009) 103532, arXiv:0902.1347 [astro-ph.HE].
[29] A. Serenelli, S. Basu, J.W. Ferguson, M. Asplund, Astrophys. J. 705 (2009) L123, arXiv:0909.2668 [astro-ph.SR]; A. Serenelli, S. Basu, J.W. Ferguson, M. Asplund, http://www.mpa-garching.mpg.de/~aldos/.
[30] J. Edsjo, WimpSim Neutrino Monte Carlo, http://www.physto.se/~edsjo/wimpsim/; M. Blennow, J. Edsjo, T. Ohlsson, J. Cosmol. Astropart. Phys. 0801 (2008) 021, arXiv:0709.3898 [hep-ph].
[31] D.V. Forero, M. Tortola, J.W.F. Valle, arXiv:1205.4018 [hep-ph].
[32] F.P. An, et al., DAYA-BAY Collaboration, Phys. Rev. Lett. 108 (2012) 171803, arXiv:1203.1669 [hep-ex]; F.P. An, et al., DAYA-BAY Collaboration, Chin. Phys. C 37 (2013) 011001, arXiv:1210.6327 [hep-ex].
[33] W.-L. Guo, Y.-L. Wu, Nucl. Phys. B 867 (2013) 149, arXiv:1103.5606 [hep-ph].